

Evaluation of Co/SSZ-13 Zeolite Catalysts Prepared by Solid-Phase Reaction for NO-SCR by Methane

Rania Charrad,^[a] Hanna E. Solt,^{*,[b]} József Valyon,^[b] László Trif,^[b] Faouzi Ayari,^[a, c] Mourad Mhamdi,^[a, d] Jenő Hancsók,^[e] and Ferenc Lónyi^[b]

Co/SSZ-13 zeolites were prepared by heating the finely dispersed mixture of NH₄-SSZ-13 and different cobalt salts up to 550 °C. Investigations by thermogravimetry – differential scanning calorimetry – mass spectrometry provided new insight into details of the solid-state reaction. Formation of Co carrying hydrate melt or volatile species was shown to proceed from chloride, nitrate, or acetylacetonate Co precursor salts upon thermal treatment. This phase change allows the transport of the Co species into the zeolite pores. The reaction of the NH₄⁺ or H⁺ zeolite cations and the mobile Co precursors generates

vapor or gas products, readily leaving the zeolite pores, and cobalt ions in lattice positions suggesting that solid-state ion-exchange is the prevailing process. The obtained catalysts are of good activity and N₂ selectivity in the CH₄/NO-SCR reaction. The thermal treatment of acetate or formate salts give solid intermediates that are unable to get in contact and react with the cations in the zeolite micropores. These catalysts contain mainly Co-oxide clusters located on the outer surface of the zeolite crystallites and have poor catalytic performance.

1. Introduction

Selective catalytic reduction of nitrogen oxides to N₂ with methane (CH₄/NO-SCR) has attracted much attention and has been described as a potential method for removing NO_x from the exhaust of engines, fueled by natural gas, such as lean-burn gas engines in cogeneration (CHP) systems.^[1] Cobalt-exchanged zeolites, such as Co-ZSM-5 and Co-mordenite zeolites were

shown to exhibit good activity and selectivity,^[2–5] however, their thermal and hydrothermal stability was not satisfactory for long-term practical application.^[6,7] The objective of the present work was to prepare better catalysts by introducing active Co-species into thermally and hydrothermally extremely stable SSZ-13 zeolite.^[8]

The amount of cations, exchangeable into zeolites by aqueous-phase ion exchange (APIE) is limited by the thermodynamic equilibrium of the exchange process. Even at low concentrations the Co²⁺ ions form ion pairs and bulky aqua complex that does not favor the formation of Co-rich zeolite forms.^[9–11]

In the solid-phase reaction, often referred to as solid-state ion exchange (SSIE), the temperature of finely dispersed mixture of zeolite and cobalt salt is increased to induce the reaction of the components. Using this method cobalt can be introduced into the zeolite in a single step. Some experiments show that high degree of ion exchange can be reached.^[9,11–13] The exchange level is attributed to the non-equilibrium nature of the process due to the volatile side product of the exchange reaction. For instance, if chloride salt is mixed with the acidic form of the zeolite (H-zeolite) HCl is formed that leaves the solid as gas.^[9] Further advantage of the SSIE method is that, unlike to the APIE method, no transition-metal-containing waste solution is emitted. It should be noted, however, that the metal incorporation by the zeolite material is often not complete and/or not all of the Co introduced occupy ion-exchange positions in the zeolite.^[9,12] A variety of Co salts, such as chloride, nitrate, acetate, etc. were suggested as potential precursors for SSIE;^[9,12,14] however, the chemistry and the detailed processes are usually not well established, which makes the success of the ion-exchange process unpredictable.

In this work the influence of the cobalt salt anion on the mechanism of the SSIE process and the cobalt species formed during the SSIE was investigated in details and was related to

[a] R. Charrad, Dr. F. Ayari, Dr. M. Mhamdi
Laboratoire de Chimie des Matériaux et Catalyse, Faculté des Sciences de Tunis
Université Tunis El Manar
Tunis (Tunisie)

[b] Dr. H. E. Solt, Dr. J. Valyon, L. Trif, Dr. F. Lónyi
Institute of Materials and Environmental Chemistry
Research Centre for Natural Sciences
Magyar tudósok körútja 2
1117 Budapest (Hungary)
E-mail: solt.hanna@ttk.hu

[c] Dr. F. Ayari
Faculté de Pharmacie de Monastir, Laboratoire de développement chimique, galénique et pharmacologique des médicaments
Université de Monastir
Rue Avicenne
5000 Monastir (Tunisie)

[d] Dr. M. Mhamdi
Institut Supérieur des Technologies Médicales de Tunis
Université Tunis El Manar
Tunis (Tunisie)

[e] J. Hancsók
Institute of Chemical and Process Engineering
University of Pannonia
Egyetem utca 10
8200 Veszprém (Hungary)

Supporting information for this article is available on the WWW under <https://doi.org/10.1002/open.202000239>

© 2020 The Authors. Published by Wiley-VCH GmbH. This is an open access article under the terms of the Creative Commons Attribution Non-Commercial NoDerivs License, which permits use and distribution in any medium, provided the original work is properly cited, the use is non-commercial and no modifications or adaptations are made.

the catalytic properties of the so received Co/SSZ-13 preparations in the CH₄/NO-SCR reaction. The hydrothermal stability of the most promising catalysts was also tested.

2. Results

2.1. Results of the TG-DTG-DSC-MS Measurements

The experimental conditions of the TG-DTG-DSC-MS measurements were chosen to follow the synthesis conditions of the Co/SSZ-13 catalysts prepared by solid phase reactions. Note that the catalysts obtained from the NH₄-SSZ-13/Co-salt mixtures by this preparation method were designated as Co(X)/SSZ-13, where X stands for the anion of the cobalt precursor salt, namely Cl for chloride, N for nitrate, Acac for acetyl acetate, A for acetate, and F for formate (see the details in the Experimental section).

The DTG curves derived from the thermogravimetric (TG) analysis and the corresponding DSC curves measured for the parent NH₄-SSZ-13 and the different NH₄-SSZ-13/Co-salt mixtures are shown in Figure 1A and Figure 1B, respectively. The characteristic mass spectrometric (MS) traces of desorption and/or decomposition products collected in situ during the TG experiments are presented in Figures S1–S6.

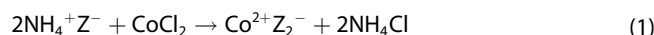
2.1.1. NH₄-SSZ-13

The parent NH₄-SSZ-13 sample presents two DTG peaks, which can be assigned to the weight loss due to water desorption from the zeolite (peak between 30–300 °C) and ammonia released during the decomposition of NH₄⁺ cations compensating zeolite framework charge (low intensity peak between

about 300–550 °C), respectively (cf. Figure 1A, a and Figure S1). The weight loss in the latter high temperature range (2.01 wt %) corresponds to 1.1 mmol/g_{cat.} NH₃ evolution, which is in good agreement with the measured NH₄⁺ ion-exchange capacity (0.95 mmol NH₃/g_{cat.}) of the NH₄-SSZ-13 sample.

2.1.2. CoCl₂·6H₂O/NH₄-SSZ-13

The DTG curve and the corresponding MS results obtained on the CoCl₂·6H₂O/NH₄-SSZ-13 mixture (Figure 1A, b and Figure S2) were similar than those measured on the parent NH₄-SSZ-13 sample (Figure 1A, a and Figure S1), except that the loss of crystalline water from the CoCl₂·6H₂O salt resulted in additional DTG peaks at 128 and 158 °C (Figure 1A, b; corresponding endothermic peaks appear at 122 and 156 °C on the DSC curve shown in Figure 1B). However, it is important to note that CoCl₂·6H₂O salt melts below 90 °C without any weight loss and the salt forms hydrate melt, i.e., a saturated solution of the hydration water.^[15,16] The solution can easily penetrate into the zeolite pores. The amount of NH₃ evolved during the thermal treatment of CoCl₂·6H₂O/NH₄-SSZ-13 mixture in the high temperature range attained about half of that obtained for the parent zeolite (cf. Figure S1 and S2), suggesting that significant fraction of the NH₄⁺ cations was exchanged by cobalt cations during the SSIE process given by Eq. 1:



(where Z⁻ represents a negatively charged segment of the zeolite). The product of the SSIE process must be NH₄Cl, which then can leave the system by sublimation into the carrier gas over about 340 °C (melting point: 338 °C, boiling point: 520 °C). Although NH₄Cl could not be detected by MS, possibly because

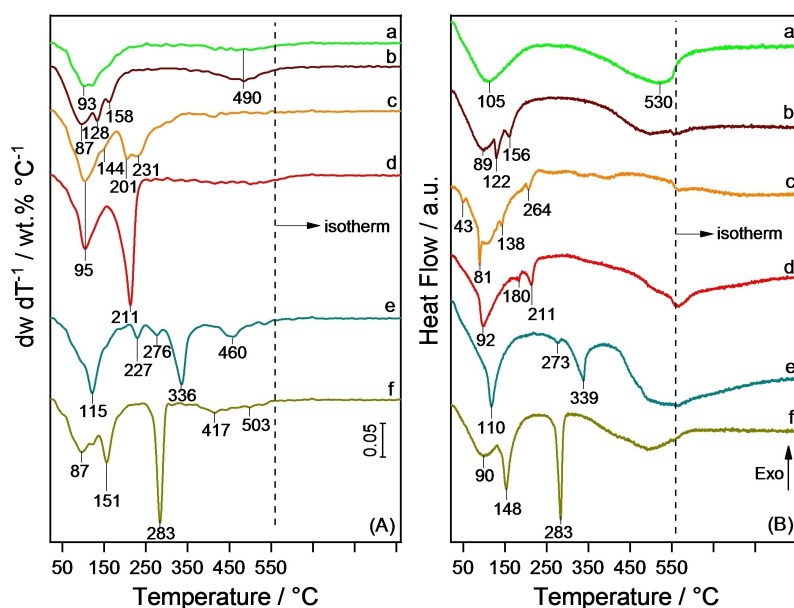
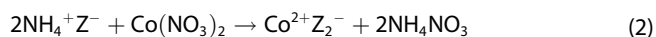


Figure 1. Curves of (A) DTG and (B) DSC of materials (a) NH₄-SSZ-13, and (b–f) physical mixture of NH₄-SSZ-13 and (b) CoCl₂·6H₂O, (c) Co(NO₃)₂·6H₂O, (d) Co(C₃H₇O₂)₂, (e) Co(CH₃COO)₂·4H₂O and (f) Co(HCOO)₂·2H₂O.

of its condensation on the lower temperature parts of the TG-DSC system, its formation is clearly supported by the weight loss (2.95 wt%) in the high temperature range (300–550 °C) that is higher than that observed for the parent $\text{NH}_4\text{-SSZ-13}$ sample (2.01 wt%) (cf. Figure 1A, a and b).

2.1.3. $\text{Co}(\text{NO}_3)_2 \cdot 6\text{H}_2\text{O}/\text{NH}_4\text{-SSZ-13}$

The DTG curve measured on the $\text{Co}(\text{NO}_3)_2 \cdot 6\text{H}_2\text{O}/\text{NH}_4\text{-SSZ-13}$ mixture shows a peak consisting of at least three components in the temperature range of 30–150 °C, which can be attributed to water desorbing from the zeolite and loss of crystalline water from the hexahydrate salt (Figure 1A, c and Figure S3). Note that $\text{Co}(\text{NO}_3)_2 \cdot 6\text{H}_2\text{O}$ melts at 55–56 °C,^[15] whereas full dehydration of the hydrate melt occurs only over about 110 °C.^[17] Formation of hydrate melt was indicated by the small endothermic peak discernible at about 43 °C on the corresponding DSC curve (Figure 1B, c). The melt of the precursor salt penetrates into the zeolite pores allowing, thereby, the SSIE to proceed. The weight loss between about 150–300 °C (Figure 1A, c) was caused by the formation of gas phase products, mainly N_2O and water, while smaller amount of NO and NO_2 also appeared in the gas phase (Figure S3). Formation of N_2O and H_2O as main products is typical for the decomposition of NH_4NO_3 ,^[18,19] which is the expected product of the SSIE process with Co-nitrate:

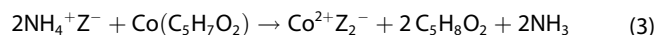


Irreversible decomposition of NH_4NO_3 to N_2O and H_2O readily proceeds at 230–260 °C,^[18] which is accordance with the characteristic temperature range observed here. Interestingly, no NH_3 evolution can be observed in the high temperature range over about 350 °C, which suggest that those NH_4^+ compensating cations, not consumed in the ion-exchange process (Eq. 2), were consumed in the reactions with the decomposition products of NH_4NO_3 (i.e. with N_2O , NO , NO_2) forming N_2 .

2.1.4. $\text{Co}(\text{C}_5\text{H}_7\text{O}_2)_2/\text{NH}_4\text{-SSZ-13}$

Heating of the $\text{Co}(\text{C}_5\text{H}_7\text{O}_2)_2/\text{NH}_4\text{-SSZ-13}$ mixture resulted in a DTG curve with two intense, somewhat overlapping peaks in the temperature ranges of 30–150 °C and about 100–250 °C (Figure 1A, d), which can be attributed to the desorption of water from the zeolite and to the formation of acetylacetone ($\text{C}_5\text{H}_8\text{O}_2$), respectively (Figure S4). Formation of ammonia is also clearly discernible in this temperature range. It should be noted, that partial volatilization of $\text{Co}(\text{C}_5\text{H}_7\text{O}_2)_2$ occurs before melting (160 °C) already between 55–130 °C^[20] and its evaporation is nearly complete at 160 °C without any noticeable decomposition.^[21] Thus, the easy volatilization allows the penetration of the Co-precursor salt into the zeolite pores. The appearance of acetylacetone and ammonia in the gas phase clearly suggests that the Co ion exchange readily proceeds in

the 100–250 °C temperature range. The formation of acetylacetone from $\text{Co}(\text{C}_5\text{H}_7\text{O}_2)_2$ requires a hydrogen transfer ($\text{C}_5\text{H}_7\text{O}_2^- + \text{H}^+ \rightarrow \text{C}_5\text{H}_8\text{O}_2$). Therefore, the ion-exchange process can be rationalized as shown by Eq. 3:



The decomposition of NH_4^+ -cations not consumed in the ion-exchange process resulted in an ammonia evolution peak in the temperature range of 350–550 °C (Figure S4).

2.1.5. $\text{Co}(\text{CH}_3\text{COO})_2 \cdot 4\text{H}_2\text{O}/\text{NH}_4\text{-SSZ-13}$

The DTG curve measured on the $\text{Co}(\text{CH}_3\text{COO})_2 \cdot 4\text{H}_2\text{O}/\text{NH}_4\text{-SSZ-13}$ mixture presents a peak in the 30–200 °C temperature range, which is due to the water desorption from the zeolite and loss of some crystalline water from the acetate salt (Figure 1A, e and Figure S5). The weight loss over about 200 °C (peaks at 227, 276, and 336 °C) are mostly due to the evolution of acetic acid, which is accompanied by the formation of acetone, CO and water over about 300 °C (Figure S5). Former studies on the thermal decomposition of $\text{Co}(\text{CH}_3\text{COO})_2 \cdot 4\text{H}_2\text{O}$ revealed that the tetrahydrate salt melts and then the crystal water is quickly evaporated in the 90–140 °C temperature range.^[22] Melting and the release of crystal water are strongly overlapping processes.^[15] The appearance of a relatively sharp peak at 115 °C on the DTG curve (at 110 °C on the DSC curve) are in accordance with this notion (Figure 1, e). It follows that the melt hydrate is quickly transformed to solid $\text{Co}(\text{CH}_3\text{COO})_2$, that hardly can move into the zeolite pores. It was also shown that formation of intermediate compounds, such as, basic Co-acetate (possibly $\text{Co}_3(\text{CH}_3\text{COO})_5\text{OH}$) and Co-acetoacetate ($\text{Co}(\text{CH}_3\text{COCH}_2\text{COO})_2$) via hydrolysis and decomposition reactions of the dehydrated and/or partially dehydrated salts readily occurs between about 200–300 °C. The decomposition is accompanied by release of gas phase acetic acid and/or water.^[22] The decomposition of the bulky Co compound intermediates generally starts over about 300 °C and finally results in the formation of CoO, while different decomposition products, such as acetic acid, acetone, carbon monoxide and carbon dioxide are released into the gas phase. The MS-traces observed over 200 °C, shown in Figure S5, clearly suggest that above processes also prevail during the heating of the $\text{Co}(\text{CH}_3\text{COO})_2 \cdot 4\text{H}_2\text{O}/\text{NH}_4\text{-SSZ-13}$ mixture. Thus, the SSIE process must be strongly hindered by the transformation of the precursor salt to bulky intermediate Co-compounds and, finally, to CoO.

2.1.6. $\text{Co}(\text{HCOO})_2 \cdot 2\text{H}_2\text{O}/\text{NH}_4\text{-SSZ-13}$

The DTG curve measured on the $\text{Co}(\text{HCOO})_2 \cdot 2\text{H}_2\text{O}/\text{NH}_4\text{-SSZ-13}$ mixture shows two main peaks at around 90 °C and 150 °C (Figure 1A, f), which can be assigned to water desorbing from the zeolite and to the loss of crystalline water from the Co-precursor salt (Figure S6).^[15,23] Note that we could not detect either HCOOH (or its decomposition products) or NH_3 , expected

to be formed at low temperature. The appearance of a sharp peak at 283 °C (Figure 1A and 1B, f) indicates a fast decomposition process, in which CO, CO₂, and water were released into the gas phase (Figure S6). Considering the characteristic peak temperature and the products formed, this process can be identified as the thermal decomposition of the dehydrated Co(HCOO)₂ precursor salt^[23,24] giving Co/CoO as final products. These results suggest, that Co(HCOO)₂ in its dehydrated form could not move into the zeolite pores in an amount, to obtain significant degree of SSIE.

2.2. Physico-Chemical Properties of the Co/SSZ-13 Catalysts

2.2.1. Crystallinity

The XRPD patterns of the parent NH₄-SSZ-13 zeolite and the Co/SSZ-13 catalysts are compared in Figure 2. Results suggest that the crystallinity of the samples was preserved during introduction of cobalt regardless of the used cobalt salt. The (311) reflection of Co₃O₄ was detectable only in the patterns of

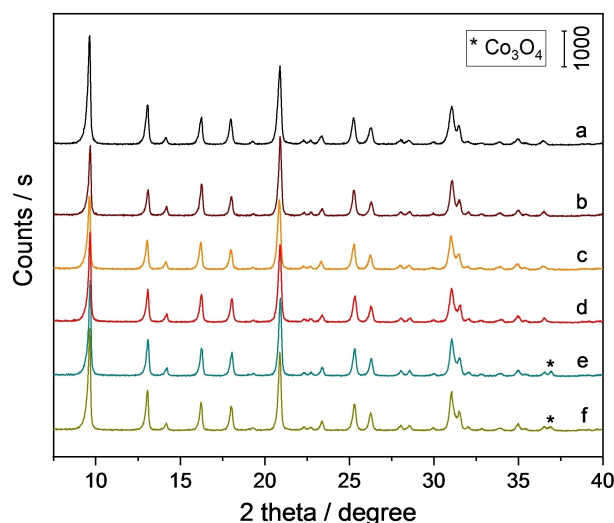


Figure 2. XRPD patterns of the (a) parent NH₄-SSZ-13, and the fresh (b) Co(Cl)/SSZ-13, (c) Co(N)/SSZ-13, (d) Co(Acac)/SSZ-13, (e) Co(A)/SSZ-13, and (f) Co(F)/SSZ-13 catalysts.

Table 1. Composition and texture.					
Sample	Co/Al _F ^a	Co wt % ^b	S _{BET} ^c [m ² g ⁻¹]	S _μ ^d [m ² g ⁻¹]	V _p ^e [cm ³ g ⁻¹]
NH ₄ -SSZ-13	–	–	696	659	0.335
Co(Cl)/SSZ-13	0.41	2.56	550 (581)	510 (527)	0.283 (0.302)
Co(N)/SSZ-13	0.38	2.42	621 (602)	573 (546)	0.326 (0.313)
Co(Acac)/SSZ-13	0.38	2.41	623 (558)	571 (507)	0.317 (0.302)
Co(A)/SSZ-13	0.31	1.94	642 (611)	594 (567)	0.324 (0.313)
Co(F)/SSZ-13	0.31	1.98	649 (622)	605 (570)	0.326 (0.314)

[a] The Al_F content was determined by ²⁹Si MAS NMR (Figure S8). [b] Determined by AAS analysis of air dry samples. [c] In parenthesis S_{BET} is given after catalytic test. [d] Microporous surface area, S_μ = S_{BET} - S_{meso}. S_{meso} was determined by the t-plot method. In parenthesis S_μ is given, determined after catalytic test. [e] Total pore volume. The V_p given in parenthesis, was determined after catalytic test.

Co(A)/SSZ-13 and Co(F)-SSZ-13 as new crystalline phase (Figure 2). Note that the comparison of the XRPD patterns taken before and after catalytic test in the presence of 5.5 vol% water vapor in the input gas stream suggest that the crystallinity of the samples was not affected during the catalytic runs (Figure S7).

2.2.2. Composition and Texture

Cobalt contents and textural properties of the Co/SSZ-13 catalysts, prepared using different Co-salts are summarized in Table 1. The chemical analysis suggested that about 10 to 30% of the cobalt was lost during the SSIE process. Similar loss of cobalt was reported by a former study.^[12] It was explained that a fraction of Co sublimated out from the mixture of the solids in the form of volatile Co compound during the SSIE process. The cobalt to framework aluminum atomic ratio (Co/Al_F) in the obtained catalysts was between 0.31 and 0.41.

Introduction of cobalt by solid-phase reaction was found to cause only relatively small (7–20%) decrease of the specific surface area (S_{BET} and S_μ) and the total pore volume (V_p) relative to the corresponding property of the parent NH₄-SSZ-13 zeolite (Table 1). The used catalysts showed nearly the same textural properties as the fresh samples suggesting that no significant structural damage occurred during the catalytic run. XRPD analysis confirmed that the crystallinity of the catalysts was retained during the solid-phase reaction and the catalytic tests (vide supra). The 40–50 m²g⁻¹ difference between the BET surface area and the microporous surface area corresponds to the surface area of the mesopores. Notice that similar surface area characterizes the mesopores of the parent NH₄-SSZ-13 sample and the catalyst preparations.

2.3. Characterization of Co-species Formed During SSIE Process

2.3.1. H₂-TPR

Peaks of H₂-TPR patterns of Co-zeolites can be assigned to reduction of specific Co species.^[5,12,25–29] It is generally agreed that Co-oxide species located on the outer surface of the zeolite crystallites and CoO_x species, including polynuclear Co-oxocations, dispersed within zeolite pores give reduction peak(s) in the temperature ranges of about 100–400 °C and 400–600 °C, respectively. Isolated Co²⁺ and [Co–OH]⁺ cations in ion-exchange positions can be reduced only over about 600 °C. It was shown that the strength of cation-to-framework interaction strongly affects the reducibility of the cations.^[25,28] The temperature of a H₂-TPR peak that corresponds to the reduction of a cationic Co species depends on the strength of stabilization. The H₂-TPR curves obtained for Co(A)/SSZ-13 and Co(F)/SSZ-13 suggest that these samples contain predominantly cobalt species reducible below 500 °C. These species must be cobalt oxides (Figure 3, d and e). The most intense reduction peaks around 370 °C indicate that majority of cobalt oxides formed

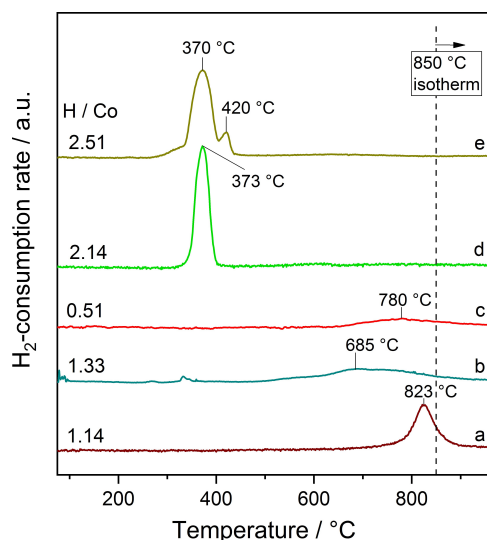


Figure 3. H₂-TPR curves of fresh (a) Co(Cl)/SSZ-13, (b) Co(N)/SSZ-13, (c) Co(Acac)/SSZ-13, (d) Co(A)/SSZ-13, and (e) Co(F)/SSZ-13 catalysts.

are located on the outer surface of the zeolite crystallites. The H/Co atomic ratio, calculated from the hydrogen consumption and the cobalt content of the sample, was 2.14 for Co(A)/SSZ-13, and 2.51 for Co(F)/SSZ-13. Both values are between 2.0 and 2.67 which would correspond to the full reduction of CoO and Co₃O₄, respectively. This infers that the majority of cobalt in these samples contains CoO and Co₃O₄ in different proportions. These results are in agreement with the XRPD measurements, which confirmed the presence of crystalline Co-oxide in Co(A) and Co(F)/SSZ-13 samples (Figure 2).

In contrast, the Co(Cl)/SSZ-13, Co(N)/SSZ-13, and Co(Acac)/SSZ-13 samples contain only hard-to-reduce cobalt species giving reduction peaks well above 600 °C (Figure 3, a–c), which can be attributed to the reduction of isolated lattice cobalt cations of the zeolite, such as Co²⁺ and [Co–OH]⁺. The full reduction of these ionic cobalt species requires two hydrogen atoms per Co atom. The obtained H/Co ratios are far below 2.0 indicating that 43.0%, 33.5%, and 74.5% of the total cobalt content in the Co(Cl)/SSZ-13, Co(N)/SSZ-13, and Co(Acac)/SSZ-13 samples, respectively, are not reducible below and at 850 °C. Extremely hard-to-reduce Co species were often observed in Co-zeolites.^[12,25–27,29] The low reducibility suggests that the Co²⁺ ions are in lattice locations, where they are tightly surrounded by oxide ions of the zeolite framework and/or the lack of near neighbor cobalt atoms that could participate in energetically favored formation of metal-metal bonds.^[26,27,30]

2.3.2. UV-Vis DRS

Results of the H₂-TPR measurement suggested that, depending on the used Co precursor salt, the obtained Co/SSZ-13 sample contains either isolated cobalt cations or cobalt oxides as dominant species (vide supra). The lattice cobalt cations in dehydrated state were shown to give characteristic bands in

the 12500–30000 cm⁻¹ region in the UV-Vis spectrum, whereas the Co-oxides give no signal in this spectral range.^[28,31]

The UV-Vis spectrum of the Co(Cl)/SSZ-13 sample (Figure 4, a), containing cobalt mainly in ion-exchange positions (as revealed by H₂-TPR) presents several component bands in the 12500–30000 cm⁻¹ region attributable to d-d transitions of Co (II) ions. Detailed assignment of the component bands in similar Co/SSZ-13 samples was carried out by Mlekodaj et al.^[31] The assigned component bands are indicated in Figure 4. The component bands attributed to cobalt ions located in 8-member rings (8MR, τ sites; 15000; 16100; 17000; 20500 cm⁻¹), regular 6-member rings (6MR, σ sites; 24500; 27000 cm⁻¹) and hexagonal prisms (ω sites; 18500; 21500 cm⁻¹) can be clearly distinguished in the spectra of the Co(Cl)/SSZ-13 samples (Figure 4, a). The spectrum measured on the used Co(Cl)/SSZ-13 catalyst indicate a slight redistribution of cobalt ions (Figure 4, a, dashed line). In contrast, no absorption bands in the 12500–27000 cm⁻¹ spectral range are discernible in the spectra of the Co(F)/SSZ-13 catalyst (Figure 4, b), which was shown to contain predominantly Co-oxides located on the outer surface of the zeolite crystallites. These results are in full agreement with the results of the H₂-TPR measurements (vide supra).

2.4. FTIR Spectroscopy

2.4.1. The ν_{OH} region

IR spectra of H-SSZ-13 and the Co/SSZ-13 samples in the ν_{OH} region are shown in Figure 5A. The band at 3736 cm⁻¹ corresponds to isolated silanol (Si–OH) groups located on the external zeolite surface,^[32] whereas the band at around 3665 cm⁻¹ stems from OH-groups attached to extra-framework

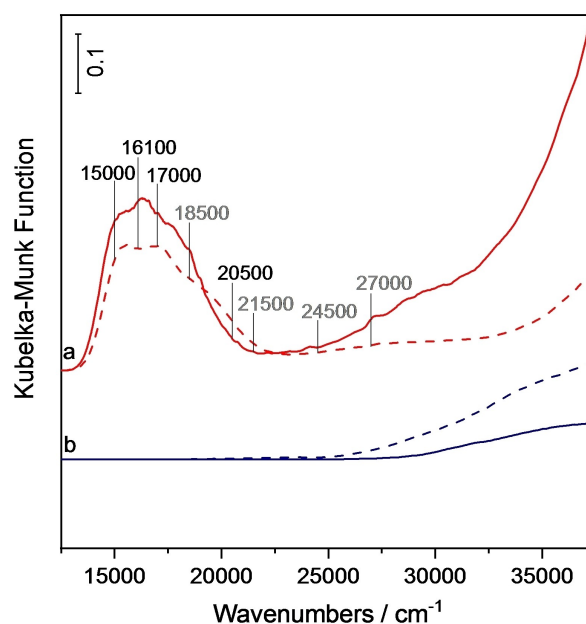


Figure 4. UV-Vis DRS spectra of (a) Co(Cl)/SSZ-13 and (b) Co(F)/SSZ-13 catalysts before (solid lines) and after (dashed lines) CH₄/NO-SCR catalytic run. Spectra were collected in He flow at 550 °C.

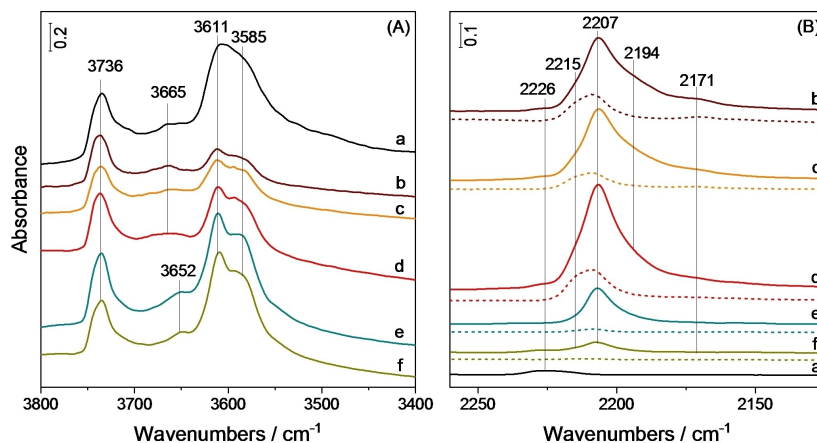


Figure 5. FTIR spectra of (A) the $\nu(\text{OH})$ region for samples (a) H-SSZ-13, (b) Co(Cl)/SSZ-13, (c) Co(N)/SSZ-13, (d) Co(Acac)/SSZ-13, (e) Co(A)/SSZ-13, and (f) Co(F)/SSZ-13; and (B) difference spectra of the $\nu(\text{CO})$ region after contacting the corresponding samples with CO at 5 mbar CO pressure at room temperature for 30 min (solid lines) and then after 5 min evacuation (dashed lines). Before measurements pellets were activated by evacuation at 500 °C for 1 h. All the spectra were recorded at room temperature. The spectra of adsorbed CO were obtained as difference of the spectra collected before and after CO adsorption

aluminum species.^[33] The intensity of this latter band is similar before (Figure 5A, a) and after cobalt introduction (Figure 5A, b–f), confirming that the ion-exchange procedure did not cause noticeable dealumination of the zeolite framework. The pair of bands at 3611 and 3585 cm^{-1} (Figure 5A, a) shows the presence of two families of Brønsted acid bridging OH-groups (Si–OH–Al) characteristic for H-SSZ-13 zeolites.^[33] The higher and the lower frequency bands belong to Brønsted acid hydroxyl groups in the 8MR and the 6MR, respectively. The lower intensity of latter bands in the spectra of the Co(Cl)/SSZ-13, Co(N)/SSZ-13, and Co(Acac)/SSZ-13 samples (Figure 5A, b–d) suggests that substitution of both types of Brønsted acid protons occurred to a significant extent by ionic Co species during the SSIE process. In contrast, these component bands (at 3611 and 3585 cm^{-1}) mostly retained their intensities in the Co(A) and Co(F)/SSZ-13 samples (Figure 5A, e and f), indicating that the Co ion-exchange hardly proceeded in these latter samples.

2.4.2. Spectra of Adsorbed CO

The weak Lewis base CO can interact with Lewis acid sites, like Co^{2+} ions. Brønsted acid sites usually adsorb CO in detectable amount only at low temperature, e.g., at or below $-100\text{ }^{\circ}\text{C}$ or at elevated pressure. Due to the polarization of CO during these interactions, the C–O stretching frequency is shifted from that of the free molecule (2143 cm^{-1}) to a characteristic frequency,^[34] which makes CO to an ideal molecule to probe electrostatic fields around Lewis and Brønsted acid sites by means of IR spectrometry.

As expected, the adsorption of CO did not affect the $\nu(\text{OH})$ bands (not shown), which is in line with former observation that acidic OH-groups cannot retain CO in detectable amount at room temperature.^[35] The very weak $\nu(\text{CO})$ band at 2226 cm^{-1} (Figure 5B, a) can be attributed to CO bound to Lewis acid extra-framework aluminum species, such as $[\text{AlO}]^+$ species.^[32,36] Similar band appears also in the corresponding

spectra obtained for the Co/SSZ-13 samples (Figure 5B, b–f). This band exists only in the presence of CO gas in the IR cell and quickly disappears upon evacuation of the cell at room temperature (Figure 5B, dashed lines). Because this is the only band obtained from the adsorption of CO over H-SSZ-13 zeolite any other band appearing in the spectrum of the catalysts must arise from CO bound to Co species.

The highest intensity spectral feature of Co-bound carbonyls consists of a main band at 2207 cm^{-1} and three well discernible component bands appearing as shoulders on its high (2215 cm^{-1}) and low frequency side (2194 and 2171 cm^{-1}), respectively (Figure 5B, b–f). Similar strong carbonyl band have been observed in the 2204–2208 cm^{-1} frequency range on different Co-zeolites, however, the assignment is still a matter of debate.^[5,35–40] Some research groups attributed this band to Co^{3+} –CO species,^[35,38] whereas others argued that Co^{3+} does not form carbonyls^[5,37] and this band should be assigned to CO attached to Co^{2+} in exchangeable lattice cation positions. The corresponding band at 2207 cm^{-1} has the highest intensity in all of our Co/SSZ-13 samples. Since the SSIE was carried out in inert atmosphere, the oxidation of Co^{2+} -ions in the Co(II) precursor salts to Co^{3+} is not expected as it requires the presence of oxygen and high temperature ($>450\text{ }^{\circ}\text{C}$) to occur in significant extent.^[41] Therefore, we assign the band at 2207 cm^{-1} to carbonyl species formed on Co^{2+} lattice cations of zeolite SSZ-13.

The band at 2194 cm^{-1} was assigned either to CO bond to Co^{2+} in oxide-like species^[5,37] or to Co^{2+} lattice cations located in relatively narrow zeolite cages.^[39,42] Since the results of the UV-Vis DRS and H_2 -TPR measurements indicated the presence of hard-to-reduce Co^{2+} species as dominating form of Co in the catalysts prepared with chloride, nitrate, or acetylacetonate precursor, the most intense component bands, both at 2207 and 2194 cm^{-1} (Figure 5B) were assigned to Co^{2+} –CO carbonyl species. Two similar overlapping component bands were obtained from CO adsorption over Co-mordenite catalysts.^[39] They were attributed to carbonyls of Co^{2+} ions located in the

main channels (the higher frequency component band) and in the side pockets (the lower frequency component band) of the mordenite structure, respectively. Szanyi et al.^[42] also observed a similar pair of CO bands studying Fe-SSZ-13 samples and attributed them to carbonyls formed on Fe^{2+} ions located in the 8MR (the higher frequency component band) and in the 6MR (the lower frequency component band) of the chabazite structure, respectively. Based on these results, we assign the bands at 2207 and 2194 cm^{-1} to carbonyls formed on Co^{2+} species located at two different cationic positions of the zeolite structure, namely in the 8MR and the 6MR, respectively. Note that the high frequency component band at 2207 cm^{-1} was more resistant to evacuation than the low frequency band at 2194 cm^{-1} (Figure 5B, b-d, dashed lines). This observation is in line with earlier findings^[39,42] and clearly supports our above assignment.

The weak carbonyl band at 2215 cm^{-1} (Figure 5B) can be attributed to carbonyl species formed on Co-oxo-cations.^[39,40] Both Co^{2+} ions in $[\text{Co}(\text{II})-\text{O}-\text{Co}(\text{II})]^{2+}$ species^[39] and Co^{3+} ions in $[\text{Co}(\text{III})\text{O}]^+$ and polynuclear $[\text{Co}_x\text{O}_y]^{n+}$ species^[40] were suggested as possible adsorption sites. Since our catalyst preparations were made in inert atmosphere, the involvement of $[\text{Co}(\text{II})-\text{O}-\text{Co}(\text{II})]^{2+}$ species seems to be the most likely. Three weak bands appeared in the 2120–2020 cm^{-1} region of the spectra of Co(Cl)/SSZ-13, Co(N)/SSZ-13, and Co(Acac)/SSZ-13 samples being in contact with CO at 5 mbar CO pressure at room temperature. The bands are assignable to $\text{Co}^+(\text{CO})_2$ and $\text{Co}^+(\text{CO})_3$ species (bands at (2114, 2040 and 2093 cm^{-1})^[39,40] (Figure S9). These bands indirectly affirm the presence of $[\text{Co}-\text{O}-\text{Co}]^{2+}$ species in these samples, since CO can reduce Co^{2+} to Co^+ at low temperature only in these oxo-cations.^[39,40]

Note however, that the corresponding Co-oxo-cations represent only a minor fraction of Co-species beside the most abundant Co^{2+} species.

A band, not totally disappearing upon evacuation of the IR cell, is discernible at around 2170 cm^{-1} (Figure 5B, b-f). A similar carbonyl band was obtained by Busca et al.^[43] from the adsorption of CO over CoAl_2O_4 spinel. The band was attributed to CO adsorbed on octahedral Al^{3+} sites in spinel structure. In our catalysts minor amount of CoAl_2O_4 might have been formed in the high-temperature solid-phase reaction of extra framework Al species and cobalt salt.

The results of the CO adsorption experiments confirm that, in line with H_2 -TPR and UV-Vis DRS results, the Co/SSZ-13 catalysts, prepared with chloride, nitrate, or acetylacetonate Co-precursors contain mainly lattice Co^{2+} cations. In contrast, samples obtained by SSIE using acetate or formate do not contain similar Co species in significant amount.

2.4.3. NO-SCR Activity

Using inert quartz wool in the reactor, NO was converted to NO_2 in the whole temperature range (300–700 °C) at a maximum conversion level of about 6% (Figure S10). The lack of N_2 formation suggests that the NO-SCR reaction does not proceed without a catalyst. Very similar conversion curves were obtained over the catalysts prepared using the chloride, nitrate, or acetylacetonate salt of cobalt (Figure 6 A–C). Above 450 °C the reaction proceeded very selectively towards the formation of N_2 . Only negligible amount of NO_2 could be detected in the product mixture. In contrast, significantly higher NO_2 formation

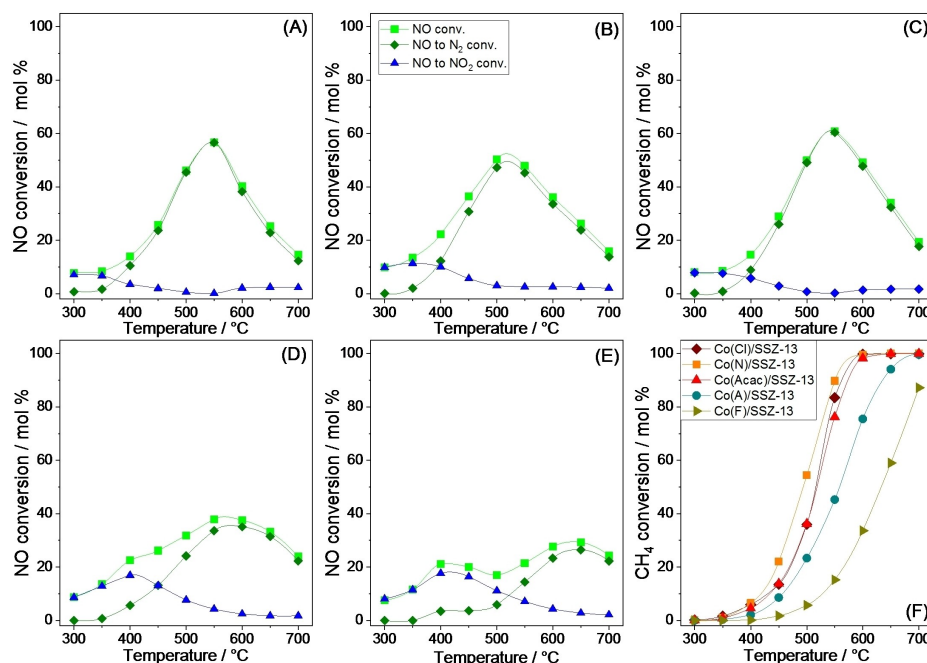


Figure 6. Conversion of (A–E) NO in the NO-SCR reaction over (A) Co(Cl)/SSZ-13, (B) Co(N)/SSZ-13, (C) Co(Acac)/SSZ-13, (D) Co(A)/SSZ-13, and (E) Co(F)/SSZ-13. Section (F) shows the conversion of CH_4 in these reactions. The reactant flow was 4000 ppm NO/4000 ppm CH_4 /2% O_2 /He, the GHSV was 30,000 h^{-1} . Before reaction, the catalysts were treated in situ in He flow at 700 °C for 1 h. For catalytic activity reported as turnover frequency see Table S1.

could be observed over the Co(A)/SSZ-13 and Co(F)/SSZ-13 catalysts at temperatures below 500 °C, whereas the reaction become selective for N₂ formation only over about 600 °C (Figure 6 D–E). Table S1 reports the catalytic activity of the samples as turnover frequencies (TOF).

Since the combustion exhausts contain water vapor in high concentration, tests were carried out to study the effect of steam on the catalytic activity and hydrothermal stability of the best NO-SCR catalysts. Alternately dry and wet reactant mixture was fed on the catalyst and the activity was monitored (Figure 7).

In the presence of water vapor both NO and CH₄ conversions decreased relative to those obtained with dry reactant over all the catalysts. However, methane conversion decreased to a substantially higher extent than the conversion of NO to N₂. It follows that the presence of water vapor suppressed mainly the consumption of methane in the undesired methane combustion reaction (Eq. 4), whereas the main reaction leading to N₂ formation (Eq. 5) was less affected.

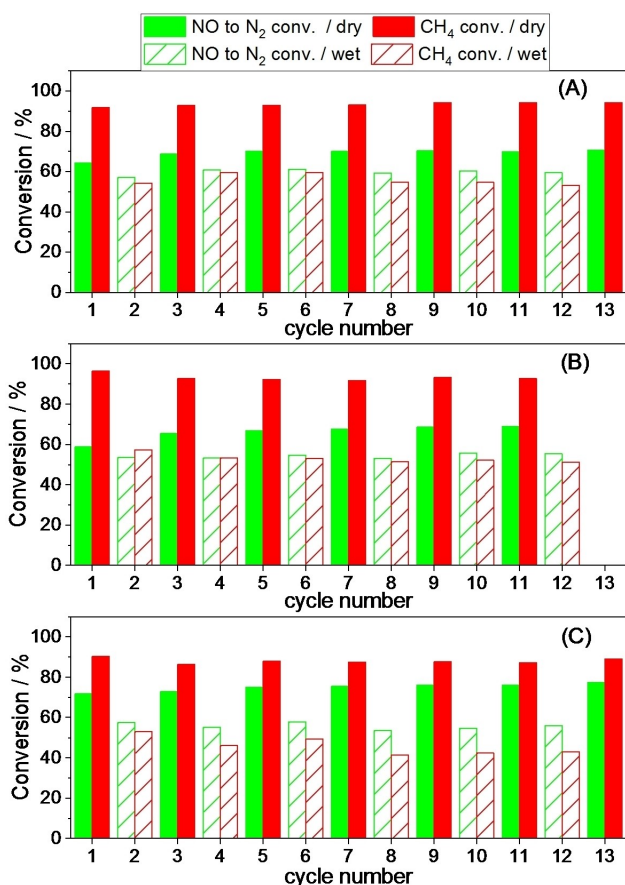
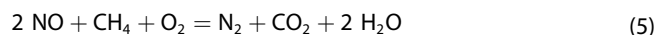


Figure 7. Effect of water on the CH₄/NO-SCR activity of (A) Co(Cl)/SSZ-13, (B) Co(N)/SSZ-13, and (C) Co(Acac)/SSZ-13. Dry reaction mixture contained 3000 ppm NO, 4000 ppm CH₄, and 2% O₂ in He, whereas wet reaction mixture contained additional 5.5 vol% H₂O on the expense of balance helium. Reaction was carried out at 550 °C and at GHSV of 15,000 h⁻¹ alternating dry and wet feed. Bars show the conversion of NO to N₂ (green bars) and the conversion of CH₄ (red bars) measured using dry reaction mixture (full bars, odd cycle numbers) and wet reaction mixture (grafted bars, even cycle numbers). The dry and wet reaction conditions were maintained for 40–40 min.



The more pronounced effect of water on the methane combustion reaction is shown by the CH₄-selectivity index (α), which indicate the fraction of converted CH₄, used to reduce nitric oxide to nitrogen^[44] (Eq. 6).

$$\alpha (\%) = \frac{0.5 \times [\text{NO}]_0 \times X_{\text{NO} \rightarrow \text{N}_2}}{[\text{CH}_4]_0 \times X_{\text{CH}_4}} \times 100 \quad (6)$$

where [NO]₀ and [CH₄]₀ stands for the concentrations of NO and CH₄ in the reactor input gas, X_{NO→N₂} for the conversion of NO to N₂ (mol %), and X_{CH₄} for the total conversion of CH₄ (mol %). The constant 0.5 in Eq. 6 comes from the stoichiometric ratio of methane to nitric oxide in Eq. 5. The higher α indices observed under wet reaction conditions imply that in the presence of water mainly the methane consumption in the undesired combustion side reaction was suppressed (Table 2). It is worth to note that the effect of water was reversible and the catalysts showed stable activity during the applied 12–13 cycles.

3. Discussion

3.1. The SSIE Process and the Nature of Co Species Formed

The SSIE method involves heating finely powdered mixture of a zeolite, being preferably in H⁺ or NH₄⁺ cationic form, and a metal salt to make the metal ion to take over the charge balancing function of lattice cations.^[10,13] In former studies a variety of Co salts were used to introduce cobalt cations into zeolites by SSIE with more or less success;^[9,11,12,14,45] however, the underlying reasons behind the success or failure of getting Co-zeolite with or without Co²⁺ lattice cations were not fully understood. The objective of the present study was to better understand the chemistry of the SSIE process with different salts of cobalt to get Co/SSZ-13 catalyst. The NH₄⁺ form of SSZ-13 zeolite was used to hinder the formation of acid product from the anion of the salt that could damage of the zeolite structure. The SSIE with cobalt chloride, nitrate, and acetylacetonate resulted in Co/SSZ-13 zeolite containing cobalt ions predominantly in ion-exchange positions. In contrast, the use of acetate or especially formate salt led mostly to formation of Co-

Table 2. Conversion of NO to N₂ and the CH₄-selectivity index (α) under dry and wet reaction conditions

Sample	NO to N ₂ conversion, % ^[a]		CH ₄ selectivity index (α), % ^a	
	dry	wet	dry	wet
Co(Cl)/SSZ-13	70.2	60.6	28.0	40.0
Co(N)/SSZ-13	68.4	54.7	27.6	39.5
Co(Acac)/SSZ-13	76.5	55.4	32.4	47.3

[a] Average values calculated from the data shown in Figure 7.

oxide, clustering on the outer surface of the zeolite crystallites. Obviously, the result of the reaction depends on a number of factors, such as, the melting temperature and vapor pressure of the salt, the way of salt decomposition, and the diffusivity of the Co carrying species in the zeolite pores.^[9,11,12,26,41,46]

Our results show that the SSIE readily proceeds, if the Co precursor salt can reach the exchangeable lattice cations, react with them inside the zeolite crystallites and the product(s) formed from the anion of the salt can leave the pores as vapor or gas. The hexahydrate of Co-chloride and nitrate melts at relatively low temperature (<100 °C) forming a saturated solution of the Co-compound in the hydration water of the crystal. The solution readily seeps into the zeolite micropores. The exchange reaction of the chloride precursor and the NH₄⁺ lattice cations results in the formation of Co-zeolite and NH₄Cl. The NH₄Cl does not decompose, but leaves the pores by sublimation/evaporation at temperatures above about 340 °C. The product of the reaction with nitrate salt are Co-zeolite and NH₄NO₃, which readily decomposes in the 150–300 °C temperature range. The leaving products are mainly N₂O and H₂O gases. Interestingly, in former studies the SSIE was found not to proceed well using nitrate salt and H-form zeolite.^[12,45] This might be due to the formation of HNO₃ during the SSIE process, which is probably an unfavorable leaving product.

Using Co-acetylacetonate the SSIE proceeds easily because this salt volatilizes at low temperature (between 55–130 °C). The vapor moves easily into the zeolite pores. Acetylaceton and NH₃ appears in the 100–250 °C temperature range as leaving product indicating proton transfer from the zeolite to the acetylacetonate ligand during the ion exchange process.

Minor amount of ionic cobalt species got in zeolite lattice positions from acetate salt. Significant amount of Co-oxide species was formed on the outer surface of the zeolite crystallites. The relatively low degree of ion-exchange can be due to simultaneous melting and dehydration of the tetrahydrate salt and/or to the transformation of the (partially) dehydrated precursor salt to bulky intermediates, most probably to Co₃(CH₃COO)₅OH and Co(CH₃COCH₂COO)₂. The transport of these bulky intermediate products, as well as the dehydrated precursor salt into the zeolite pores is strongly hindered. Their decomposition readily occurs between about 200–300 °C and produces Co-oxide species on the outer surface of the zeolite crystallites.

The SSIE process with the formate salt also resulted in minor cobalt exchange and excessive formation of Co-oxide on the outer surface of the zeolite crystallites. The virtual absence of HCOOH and NH₃ in the reaction effluent suggests that no noticeable Co ion-exchange occurred. The Co(HCOO)₂·2H₂O precursor salt becomes quickly dehydrated at around 150 °C. The decomposition of the salt at about 280 °C, leaving Co/CoO clusters on the outer surface of the zeolite crystallites. In the catalyst treated at high temperature (700 °C) in inert gas, clusters of Co₃O₄ were detected by H₂-TPR.

3.2. Relations Between the CH₄/NO-SCR Activity and the Co-Species Formed by SSIE

Former studies showed that the zeolite structure and composition and the conditions of catalyst preparation determine the catalytic activity and selectivity of Co-zeolites in the CH₄/NO_x-SCR reaction.^[3,5,6,26,27,47,48] Present study shows that the Co salt used in SSIE process also affects the properties of the formed Co sites and thus the deNO_x behavior of the catalyst.

The opinions about the role of the Co²⁺ ions in the CH₄/NO_x-SCR reaction are not fully consistent.^[4–6,26,39,47,49,50] There are ample of evidence that the N₂-forming reaction proceeds on Co²⁺ ions in ion-exchange positions of zeolite. Catalytic results shown in the present work are in agreement with this notion. The catalyst samples containing Co²⁺ ions in lattice position as dominant Co-species showed relatively good activity and selectivity towards N₂ formation (Figure 6, A–C).

In contrast, the catalyst samples, containing mainly Co-oxide clusters mainly on the outer surface of the zeolite crystallites, show activity in the oxidation of NO to NO₂. The NO₂ was the dominating product up to about 500 °C (Figure 6, D,E). These results are in line with former observations that oxide like species inside the zeolite channels or Co-oxide clusters formed outside the zeolite crystallites brings about the oxidation of NO to NO₂ that is important intermediate of the NO-SCR process.^[3,26,49] Interestingly, as reaction temperature was increased, increasing N₂ formation was observed over the Co(A)/SSZ-13 or Co(F)/SSZ-13 catalysts, containing Co²⁺ ions in very low concentration. Nitrogen was selectively formed over about 600 °C. The NO₂ is absent from the product mixture, if the rate of the NO₂-consuming N₂-forming reaction is higher than the rate of the NO to NO₂ oxidation reaction.^[3] At low concentration of Co²⁺ sites this situation probably prevails only in the high temperature range (over about 600 °C), where thermodynamics allows anyhow lower NO₂ concentrations. In the lack of Co²⁺ sites nitrogen formation may still occur in the reaction of NO₂ and CH₄ over Brønsted acid sites as it was demonstrated by Lukyanov et al.^[51] Nevertheless, Brønsted acid sites are much less active than Co²⁺ sites. At high temperature (>600 °C) the reaction over the acid sites can also contribute to the N₂-formation.

4. Conclusions

The type of the Co precursor salt used for the preparation of Co/SSZ-13 zeolite catalyst by solid-state reaction strongly affects the structure of the introduced Co-species and, thus, the activity and selectivity of the catalyst in the CH₄/NO-SCR reaction. The formation of Co carrying hydrate melt or volatile species was shown to proceed from chloride, nitrate, or acetylacetonate Co precursor salts upon thermal treatment. This phase change allows the transport of the Co species into the zeolite pores. The reaction of the H⁺ or NH₄⁺ zeolite cations and the mobile Co precursors generates vapor or gas products, readily leaving the zeolite pores, and cobalt ions in lattice positions. The obtained catalysts are of good activity and N₂ selectivity in the

CH₄/NO-SCR reaction. The thermally effected transformation of acetate or formate salts give solid intermediates that are unable to get in contact and react with the cations in the zeolite micropores. The catalyst contains mainly Co-oxide clusters located on the outer surface of the zeolite crystallites. These catalysts, show high activity in the NO reaction by O₂ to get NO₂. Over latter catalysts the NO-SCR reaction becomes selective for N₂ only at high temperatures (> 600 °C), where the NO₂ formation becomes thermodynamically limited. Under such conditions the N₂-forming reaction can consume the full amount of the forming NO₂ intermediate. At high temperatures the N₂-forming reaction between NO₂ and CH₄ on the Brønsted acid sites may also contribute to the SCR reaction.

Experimental Section

Catalyst Preparation

Na-SSZ-13 zeolite was prepared using the synthesis method described by Gao et al.^[52] A synthesis gel was prepared having a composition of 10 SDA: 10 NaOH: 4 Al₂O₃: 100 SiO₂: 2200 H₂O (Si/Al=12.5). The structure directing agent (SDA) was trimethyl adamantyl ammonium hydroxide (TMAda-OH, Sachem ZeoGen 2825). The used sodium hydroxide, aluminum hydroxide and fumed silica (particle size 7 nm) powder was obtained from Aldrich. A Teflon-lined steel autoclave, containing the synthesis gel, was kept at 160 °C for 9 days under autogenous pressure without stirring the gel. The as-synthesized zeolite product was washed with distilled water until neutral pH was reached, filtered and dried at 110 °C for 15 h. The SDA was removed from the zeolite channels by calcination in air at 550 °C for 12 h. The thus obtained Na-form SSZ-13 was transformed into NH₄⁺-form by repeating ion exchange with 1 M NH₄Cl solution (25 cm³ per g zeolite) at 70 °C three times. The product was washed to chloride free, filtered, and dried at 110 °C. The ammonium ion exchange capacity of the thus obtained parent NH₄-SSZ-13 was 0.95 mmol/g_{cat}.

Co/SSZ-13 catalyst samples were prepared using CoCl₂·6H₂O, Co(NO₃)₂·6H₂O (Merck), Co(C₃H₇O₂)₂, Co(CH₃COO)₂·4H₂O, and Co(HCOO)₂·2H₂O (Sigma-Aldrich) as Co precursor salt. The cobalt content of the final catalyst preparation was intended to be 3.1 wt%, which corresponds to a cobalt to framework aluminum atomic ratio (Co/Al_F) of 0.5 and to 100% ion-exchange level assuming Co²⁺ charge compensating cations. The amount of cobalt salt added to NH₄⁺-SSZ-13 zeolite was determined accordingly. The salt and the zeolite were thoroughly homogenized in an agate mortar for 15 min. The obtained physical mixture was heated up in helium flow at a heating rate of 2 °C min⁻¹ to 550 °C and was kept at this temperature for 12 h. It was noticed that volatile cobalt derivatives were formed that evaporated from the mixture. As a result, the final cobalt content of the catalyst preparations became less than 3 wt% (Table 1). The catalyst samples are designated as Co(Cl)/SSZ-13, Co(N)/SSZ-13, Co(Acac)/SSZ-13, Co(A)/SSZ-13, and Co(F)/SSZ-13, where the letter(s) within parenthesis refers to the anion of the used cobalt salt, namely, to chloride (Cl), nitrate (N), acetylacetonate (Acac), acetate (A), and formate (F).

Characterization

The SSIE process was studied by thermogravimetry-differential scanning calorimetry-mass spectrometry (TG-DSC-MS) technique using a Setaram Labsys Evo (Lyon, France) thermal analysis system. Finely dispersed mixtures of Co-salt and NH₄-SSZ-13 with the same

composition than that used for catalyst preparation were filled in an alumina crucible of 100 μL volume and were heated from 25 °C up to 550 °C at a heating rate of 20 °C/min, then were kept at 550 °C for one hour. The measurements were carried out in a 90 cm³ min⁻¹ flow of high purity (99.9999%) helium. The obtained differential thermogravimetric (DTG) and differential scanning calorimetric (DSC) curves were baseline corrected and further processed by the software of the system (Calisto Processing, ver. 2.06). The analysis of the evolved gases and volatiles were performed using a Pfeiffer Vacuum Omni Star™ gas analysis system (MS-EGA) connected to the TG-DSC unit. The MS was operated in electron impact mode. The temperature of the gas splitter and transfer line to the mass spectrometer was set to 220 °C. The measurement was carried out in SEM Bargraph Cycles acquisition mode, where the m/z range of 5–190 was continuously scanned at a speed of 20 ms/amu.

The cobalt and aluminum contents of the catalysts were determined by atomic absorption spectroscopy (AAS, Pro-Varian AA-20 spectrometer).

The X-ray powder diffraction (XRPD) measurements were carried out by Philips PW 1870 diffractometer using monochromatic CuKα radiation (λ=0.15418 nm). The applied generator settings were 40 kV and 35 mA, whereas the scanning rate was 0.02°/sec in the 2θ region of 3–50°.

Nitrogen adsorption/desorption isotherms were determined at –196 °C using an automated volumetric nitrogen adsorption apparatus (Surfer, Thermo Fisher Scientific) to characterize the textural properties of the samples. Samples were pre-treated under dynamic vacuum at 120 °C for 1 h and then at 250 °C for 2 h prior to the adsorption measurements. The specific surface area was determined using the BET method (S_{BET}). The t-plot method of Lippens and de Boer was used to get the micropore volume (V_μ) and the surface area of mesopores (S_{meso}). The surface area of micropores (S_μ) was obtained as the difference of S_{BET} and S_{meso}. Pore volumes (V_p) were calculated from the N₂ adsorption capacity at the relative pressure of 0.95.

The reducibility of Co species was characterized by temperature-programmed reduction with hydrogen (H₂-TPR). Sample (~70 mg, particle size: 0.25–0.5 mm) was placed into a quartz microreactor tube (I.D.=4 mm) and was pre-treated in situ in a helium flow (30 cm³ min⁻¹, 10 °C min⁻¹) at 700 °C for 1 h. After cooling in He to room temperature, sample was contacted with a 30 cm³ min⁻¹ flow of 10% H₂/N₂ and heated from 25 °C up to 850 °C at a rate of 10 °C min⁻¹. The effluent gas was passed through a dry-ice trap and a thermal conductivity detector (TCD). The hydrogen consumption was determined from the integrated area under the TPR curve using a calibration value obtained by the reduction of known amount of CuO reference material at the same parameter settings.

The Co-species in the catalysts were characterized by UV-Vis diffuse reflectance spectroscopy (UV-Vis DRS) using a Scientific Evolution 300 UV/Vis spectrophotometer (Thermo Scientific) equipped with a high temperature reaction chamber and a Praying Mantis diffuse reflectance accessory. The samples were pre-treated in situ in 30 cm³ min⁻¹ He flow at 550 °C for 1 h. The spectra were collected in He flow at 550 °C in order to ensure the dehydrated state of the samples. BaSO₄ (Alfa-Aesar, Puratronic, 99,998%) was used as reference material. The reflectance values were converted to Kubelka-Munk function, F(R_∞), using Eq. 7, where R_∞ means the reflectance from a semi-infinite layer:

$$F(R_{\infty}) = \frac{(1 - R_{\infty})^2}{2R_{\infty}} \quad (7)$$

Catalysts were characterized also by infrared spectroscopy. Spectra were recorded by type Nicolet 6700 Fourier-Transform Infrared Spectrometer (FTIR). Self-supporting pellets were prepared and pre-treated in situ in the IR cell at 500 °C under dynamic vacuum (10^{-6} mbar) for 1 h and let to cool to room temperature in vacuum. The cobalt species were characterized by the infrared spectra of adsorbed CO. Spectra were collected at room temperature (64 scans, 2 cm^{-1} resolution).

Catalytic Tests

The catalyst sample (100 mg, particle size: 0.25–0.50 mm) was placed into a quartz tube reactor (I.D. = 4 mm) and was pre-treated in a He flow ($30\text{ cm}^3\text{ min}^{-1}$) at 700 °C for 1 h. The catalytic activity was determined in the temperature range of 300–700 °C at a gas hourly space velocity (GHSV) of $30,000\text{ h}^{-1}$ (space time 0.12 s). The reactant gas mixture contained 4000 ppm NO, 4000 ppm CH_4 , and 2% O_2 in He (balance). The hydrothermal stability of the catalysts was studied at 550 °C at GHSV of $15,000\text{ h}^{-1}$ by changing the input reactant gas mixture to a wet reactant mixture containing 5.5 vol% H_2O . The input change was repeated in 40 min intervals. The wet gas was made by feeding water directly into the hot zone of the quartz reactor above the catalyst bed using a micro metering syringe pump (Infusens® 5188.21 A, MTA KUTESZ). When water was added to the reaction mixture, the total flow rate was maintained constant by decreasing the flow of the He balance and thus maintaining the partial pressures of the reactants constant.

The effluent gas of the catalytic reactor was continuously analyzed by on-line mass spectrometer (MS, VG ProLab, Fisher Scientific) by monitoring the following characteristic masses (m/z): 4 (for He), 12 (for CH_4 and CO_2), 15 (for CH_4 and NO), 18 (for H_2O), 28 (for CO_2 , CO, and N_2), 30 (for NO and NO_2), 32 (for O_2), 44 (for CO_2) and 46 (for NO_2). The concentration of CO, N_2O and NO_2 was analyzed also by an FTIR spectrometer (Nicolet 5PC) equipped with an IR Gas Cell (PIKE Technologies), kept at to 110 °C. During all catalytic tests, the formation of CO and N_2O was negligible.

The catalytic conversions were calculated as follows:

Total conversion of NO (mol %):

$$X_{\text{NO}} = \frac{[\text{NO}]_0 - [\text{NO}]}{[\text{NO}]_0} \times 100 \quad (8)$$

Conversion of CH_4 (mol %):

$$X_{\text{CH}_4} = \frac{[\text{CH}_4]_0 - [\text{CH}_4]}{[\text{CH}_4]_0} \times 100 \quad (9)$$

$[\text{NO}]_0$ and $[\text{CH}_4]_0$ stands for the concentrations of NO and CH_4 in the reactor input gas, whereas $[\text{NO}]$ and $[\text{CH}_4]$ are the concentrations of the same compounds in the reactor outlet. Results were evaluated after the catalytic system reached steady state at a given reaction temperature (when the MS signals of the components were stabilized).

$$X_{\text{NO} \rightarrow \text{N}_2} (\text{mol } \%) = \frac{[\text{NO}]_0 - [\text{NO}_2] - [\text{NO}]}{[\text{NO}]_0} \times 100 \quad (10)$$

$$X_{\text{NO} \rightarrow \text{NO}_2} (\text{mol } \%) = \frac{[\text{NO}_2]}{[\text{NO}]_0} \times 100 \quad (11)$$

In Eqs 10 and 11, $[\text{NO}_2]$ is the concentration of NO_2 measured at the reactor outlet at steady-state. Because only trace amount of N_2O

could be detected throughout the catalytic tests, the N_2O concentration was omitted from Eq 10.

Acknowledgements

This work was supported by the National Research, Development and Innovation Office of Hungary (grant numbers OTKA PD-115898 and 2018-2.1.11-TÉT-SI-2018-00011). The financial support provided by the European Union and the State of Hungary, co-financed by the European Regional Development Fund in the framework of the project No. VEKOP-2.3.2-16-2017-00013, and the support of the project of the Economic Development and Innovation Operative Program of Hungary, GINOP-2.3.2-15-2016-00053 are kindly acknowledged.

Conflict of Interest

The authors declare no conflict of interest.

Keywords: NO-SCR · solid-state ion exchange · thermochemistry · hydrothermal stability · zeolite SSZ-13

- [1] K. Shimizu, F. Okada, Y. Nakamura, A. Satsuma, T. Hattori, *J. Catal.* **2000**, *195*, 151–160.
- [2] a) Y. J. Li, J. N. Armor, *Appl. Catal. B* **1992**, *1*, L31–L40; b) A. De Lucas, J. L. Valverde, F. Dorado, A. Romero, I. Asencio, *J. Mol. Catal. A* **2005**, *225*, 47–58; c) M. C. Campa, D. Pietrogioacomi, M. Occhuzzi, *Appl. Catal. B* **2015**, *168*, 293–302.
- [3] F. Lóny, H. E. Solt, Z. Paszti, J. Valyon, *Appl. Catal. B* **2014**, *150*, 218–229.
- [4] Y. J. Li, T. L. Slager, J. N. Armor, *J. Catal.* **1994**, *150*, 388–399.
- [5] A. Bellmann, H. Atia, U. Bentrup, A. Bruckner, *Appl. Catal. B* **2018**, *230*, 184–193.
- [6] T. Montanari, O. Marie, M. Daturi, G. Busca, *Appl. Catal. B* **2007**, *71*, 216–222.
- [7] a) M. Shelef, *Chem. Rev.* **1995**, *95*, 209–225; b) Y. Traa, B. Burger, J. Weitkamp, *Microporous Mesoporous Mater.* **1999**, *30*, 3–41; c) A. M. Beale, F. Gao, I. Lezcano-Gonzalez, C. H. F. Peden, J. Szanyi, *Chem. Soc. Rev.* **2015**, *44*, 7371–7405.
- [8] a) J. H. Kwak, R. G. Tonkyn, D. H. Kim, J. Szanyi, C. H. F. Peden, *J. Catal.* **2010**, *275*, 187–190; b) D. W. Fickel, E. D'Addio, J. A. Lauterbach, R. F. Lobo, *Appl. Catal. B* **2011**, *102*, 441–448; c) J. H. Kwak, D. Tran, S. D. Burton, J. Szanyi, J. H. Lee, C. H. F. Peden, *J. Catal.* **2012**, *287*, 203–209; d) H. Y. Chen, in *Urea-SCR Technology for deNOx After Treatment of Diesel Exhausts* (Eds.: I. Nova, E. Tronconi), Springer Science and Business Media, New York, **2014**, pp. 123–147.
- [9] S. Essid, F. Ayari, R. Bulanek, J. Vaculik, E. Asedegbega-Nieto, M. Mhamdi, G. Delahay, A. Ghorbel, *Microporous Mesoporous Mater.* **2018**, *264*, 218–229.
- [10] A. V. Kucherov, A. A. Slinkin, *J. Mol. Catal.* **1994**, *90*, 323–354.
- [11] S. Essid, F. Ayari, R. Bulanek, J. Vaculik, M. Mhamdi, G. Delahay, A. Ghorbel, *Solid State Sci.* **2019**, *93*, 13–23.
- [12] M. Mhamdi, S. Khaddar-Zine, A. Ghorbel, *Appl. Catal. A* **2009**, *357*, 42–50.
- [13] H. G. Karge, H. K. Beyer, *Zeolite Chemistry and Catalysis* **1991**, *69*, 43–64.
- [14] a) R. da Cruz, A. Mascarenhas, H. Andrade, *Appl. Catal. B* **1998**, *18*, 223–231; b) M. Mhamdi, E. Marceau, S. Khaddar-Zine, A. Ghorbel, M. Che, Y. Ben Taarit, F. Villain, *Catal. Lett.* **2004**, *98*, 135–140.
- [15] *CRC Handbook of Chemistry and Physics* 60th Edition ed., CRC Press, Inc., **1980**.
- [16] S. K. Mishra, S. B. Kanungo, *J. Therm. Anal.* **1992**, *38*, 2437–2454.
- [17] C. Ehrhardt, M. Gjikaj, W. Brockner, *Thermochim. Acta* **2005**, *432*, 36–40.
- [18] G. Feick, R. M. Hainer, *J. Am. Chem. Soc.* **1954**, *76*, 4.
- [19] S. Chaturvedi, P. N. Dave, *J. Energ. Mater.* **2013**, *31*, 1–26.
- [20] F. Jasim, I. Hamid, *Thermochim. Acta* **1985**, *93*, 65–68.

- [21] R. G. Charles, P. G. Haverlack, *J. Inorg. Nucl. Chem.* **1969**, *31*, 11.
- [22] a) T. Wanjun, C. Donghua, *Chem. Pap.* **2007**, *61*, 329–332; b) E. Ingier-Stocka, A. Grabowska, *J. Therm. Anal. Calorim.* **1998**, *54*, 115–123; c) M. A. Mohamed, S. A. Halawy, M. M. Ebrahim, *J. Therm. Anal.* **1994**, *41*, 387–404.
- [23] A. A. Vecher, S. V. Dalidovich, E. A. Gusev, *Thermochim. Acta* **1985**, *89*, 383–386.
- [24] A. Gorski, A. Krasnicka, *J. Therm. Anal.* **1987**, *32*, 1243–1251.
- [25] A. Martinez-Hernandez, G. A. Fuentes, S. A. Gomez, *Appl. Catal. B* **2015**, *166*, 465–474.
- [26] X. Wang, H. Y. Chen, W. M. H. Sachtler, *Appl. Catal. B* **2000**, *26*, L227–L239.
- [27] X. Wang, H. Y. Chen, W. M. H. Sachtler, *Appl. Catal. B* **2001**, *29*, 47–60.
- [28] P. Sazama, L. Mokrzycki, B. Wichterlova, A. Vondrova, R. Pilar, J. Dedecek, S. Sklenak, E. Tabor, *J. Catal.* **2015**, *332*, 201–211.
- [29] A. V. Boix, S. G. Aspromonte, E. E. Miro, *Appl. Catal. A* **2008**, *341*, 26–34.
- [30] V. Schwartz, R. Prins, X. Wang, W. M. H. Sachtler, *J. Phys. Chem. B* **2002**, *106*, 7210–7217.
- [31] K. Mlekodaj, J. Dedecek, V. Pashkova, E. Tabor, P. Klein, M. Urbanova, R. Karcz, P. Sazama, S. R. Whittleton, H. M. Thomas, A. V. Fishchuk, S. Sklenak, *J. Phys. Chem. C* **2019**, *123*, 7968–7987.
- [32] F. Giordanino, P. N. R. Vennestrom, L. F. Lundegaard, F. N. Stappen, S. Mossin, P. Beato, S. Bordiga, C. Lamberti, *Dalton Trans.* **2013**, *42*, 12741–12761.
- [33] S. Bordiga, L. Regli, D. Cocina, C. Lamberti, M. Bjorgen, K. P. Lillerud, *J. Phys. Chem. B* **2005**, *109*, 2779–2784.
- [34] S. Bordiga, D. Scarano, G. Spoto, A. Zecchina, C. Lamberti, C. O. Arean, *Vib. Spectrosc.* **1993**, *5*, 69–74.
- [35] K. Chakarova, K. Hadjiivanov, *Microporous Mesoporous Mater.* **2009**, *123*, 123–128.
- [36] a) F. Geobaldo, B. Onida, P. Rivolo, F. Di Renzo, F. Fajula, E. Garrone, *Catal. Today* **2001**, *70*, 107–119; b) T. Montanari, O. Marie, M. Daturi, G. Busca, *Catal. Today* **2005**, *110*, 339–344.
- [37] K. Gora-Marek, B. Gil, J. Datka, *Appl. Catal. A* **2009**, *353*, 117–122; K. Gora-Marek, *Top. Catal.* **2009**, *52*, 1023–1029.
- [38] A. Mihaylova, K. Hadjiivanov, S. Dzwigaj, M. Che, *J. Phys. Chem. B* **2006**, *110*, 19530–19536.
- [39] V. Indovina, M. C. Campa, D. Pietrogiamomi, *J. Phys. Chem. C* **2008**, *112*, 5093–5101.
- [40] M. I. Shilina, T. N. Rostovshchikova, S. A. Nikolaev, O. V. Udalova, *Mater. Chem. Phys.* **2019**, *223*, 287–298.
- [41] E. M. El-Malki, D. Werst, P. E. Doan, W. M. H. Sachtler, *J. Phys. Chem. B* **2000**, *104*, 5924–5931.
- [42] J. Szanyi, F. Gao, J. H. Kwak, M. Kollar, Y. L. Wang, C. H. F. Peden, *Phys. Chem. Chem. Phys.* **2016**, *18*, 10473–10485.
- [43] G. Busca, V. Lorenzelli, V. S. Escibano, R. Guidetti, *J. Catal.* **1991**, *131*, 167–177.
- [44] Y. J. Li, J. N. Armor, *Appl. Catal. B* **1993**, *3*, L1–L11.
- [45] M. Mhamdi, E. Marceau, S. Khaddar-Zine, A. Ghorbel, M. Che, Y. Ben Taarit, F. Villain, *Z. Phys. Chem.* **2005**, *219*, 963–978.
- [46] A. Jentys, A. Lugstein, H. Vinek, *J. Chem. Soc. Faraday Trans.* **1997**, *93*, 4091–4094.
- [47] C. Chupin, A. C. van Veen, M. Konduru, J. Despres, C. Mirodatos, *J. Catal.* **2006**, *241*, 103–114.
- [48] J. Dedecek, Z. Sobalik, B. Wichterlova, *Catal. Rev. Sci. Eng.* **2012**, *54*, 135–223.
- [49] D. Kaucky, A. Vondrova, J. Dedecek, B. Wichterlova, *J. Catal.* **2000**, *194*, 318–329.
- [50] a) J. Dedecek, D. Kaucky, B. Wichterlova, *Top. Catal.* **2002**, *18*, 283–290; b) M. C. Campa, S. DeRossi, G. Ferraris, V. Indovina, *Appl. Catal. B* **1996**, *8*, 315–331; c) M. C. Campa, I. Luisetto, D. Pietrogiamomi, V. Indovina, *Appl. Catal. B* **2003**, *46*, 511–522; d) M. C. Campa, V. Indovina, *J. Porous Mater.* **2007**, *14*, 251–261; e) A. Rodrigues, P. da Costa, C. Methivier, S. Dzwigaj, *Catal. Today* **2011**, *176*, 72–76.
- [51] D. B. Lukyanov, G. Sill, J. L. Ditri, W. K. Hall, *J. Catal.* **1995**, *153*, 265–274.
- [52] F. Gao, M. Kollar, R. K. Kukkadapu, N. M. Washton, Y. L. Wang, J. Szanyi, C. H. F. Peden, *Appl. Catal. B* **2015**, *164*, 407–419.

Manuscript received: August 24, 2020

Revised manuscript received: September 16, 2020